Macromolecules

pubs.acs.org/Macromolecules
Article

Mechanics of Physically Cross-Linked Hydrogels: Experiments and Theoretical Modeling

Mohit Goswami,*,§ Agniva Dutta,*,§ Rishi Kulshreshtha, Gleb Vasilyev, Eyal Zussman,* and Konstantin Volokh*

Cite This: Macromolecules 2025, 58, 4478−4487

ABSTRACT: The remarkable ductility and enhanced toughness of metal−ligand-based hydrogels caused by physical cross-links that improve their mechanical properties have proven the efficacy of hydrogels in various engineering applications. Here, we bring the first comprehensive investigation of hydrogels under bulge testing. The multiaxial response of these materials is crucial for enhanced durability and load-bearing capability. In this study, we derive a hyperelastic constitutive model with a description of failure and validate it experimentally. The latter model is further used to analyze cavitation in these materials. This study demonstrates that incorporating imidazole−Ni^{2+} metal−ligand cross-links can significantly enhance several mechanical properties. For instance, increasing the imidazole content from 40 to 70 mol % improves the elastic modulus by 400% and the ultimate equibiaxial stress by 80%. The detailed experimental investigation reveals that the inflation of these hydrogels strongly depends on structural evolution. The current study paves the way for the development of novel experimental techniques and constitutive models to fine-tune the mechanical properties of hydrogels as per user requirements.

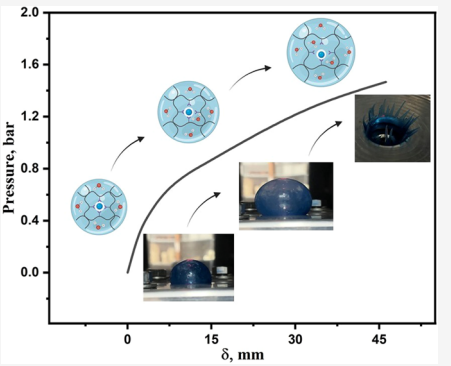

INTRODUCTION

Hydrogels are water-rich, three-dimensional cross-linked polymeric materials with promising broad applications, including electronics,[1,2] soft robotics,[3] energy storage devices,[4,5] and biomedical technologies.[6] However, synthetic hydrogels are typically fragile and lack the mechanical strength crucial for such demanding applications. As Lake and Thomas have noted, stress localization under external force causes crack initiation and premature failure.[7] Recent efforts have focused on enhancing the strength and toughness of the synthetic hydrogels by integrating energy-dissipative pathways into their structures.[4,8−10] A prominent approach is the incorporation of sacrificial bonds that preferentially break under stress, dissipating energy before the polymer backbone (primarily C−C bonds) ruptures. These sacrificial bonds are designed with association energy ($E_{\text{sacrificial bond}}$) higher than thermal energy at room temperature (k_BT) yet lower than the dissociation energy of covalent bonds (E_{C-C} ∼347 kJ/mol, or ∼140 k_BT), allowing them to withstand initial stress and delay failure.[10]

Dynamic interactions, particularly metal−ligand coordination bonds, have recently emerged as effective sacrificial bonds in the creation of tough hydrogels. Common in natural systems, coordination bonds offer versatile cross-linking for enhancing hydrogel mechanical properties. Multivalent metal ions can form stable bonds with various ligands (electron donor groups), exhibiting well-defined coordination numbers and spatial arrangements, making them invaluable for advancing hydrogel durability and functionality.

The current state-of-the-art testing methodologies used for the characterization of hydrogels include uniaxial tension tests (tensile and compression modes) and equibiaxial tests.[11,12] Furthermore, Zhang et al. performed pure shear experiments to study crack propagation in hydrogels.[13] The structural evolution of hydrogels is completely dependent on the rate of loading/unloading;[14] however, the latter variations may be observed while using different testing methodologies. Generally, the loads experienced by these materials are multiaxial when used in certain applications, which requires the development of sophisticated testing methodologies. The bulge tests have proven their efficacy in the structural analysis of a variety of soft materials.[15−17] However, the interpretation of results is not trivial due to nonuniformity in the strain distribution. Concerning the latter interpretation, the reverse finite-element (FE)-based methodologies have been quite successful in the recent past. Till now, there have been several studies concerning the constitutive modeling of hydrogels. For

Received: February 20, 2025
Revised: March 31, 2025
Accepted: April 15, 2025
Published: April 21, 2025

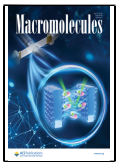

https://doi.org/10.1021/acs.macromol.5c00486
Macromolecules 2025, 58, 4478−4487

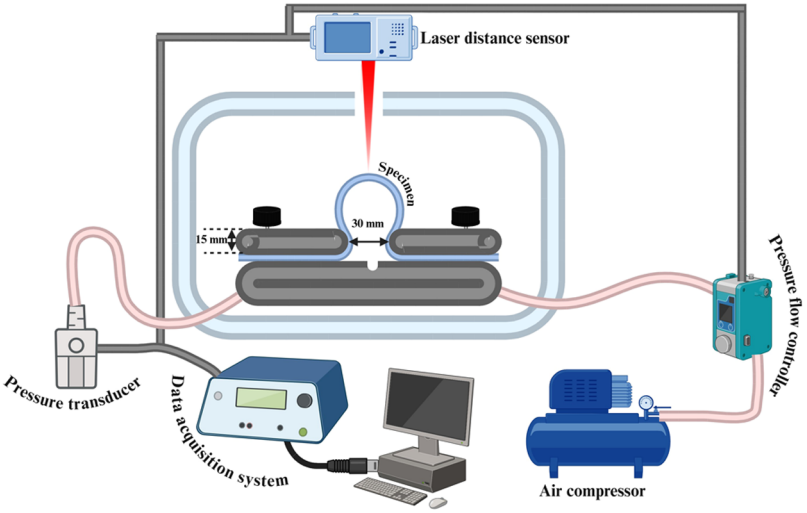

Figure 1. Schematic diagram of the bulge test device used to inflate the hydrogel specimen.

example, Levin et al. proposed a statistical mechanics-based framework based on the entropic response of molecular chains.[18] Zhong et al. proposed a hyperviscoelastic model based on varied water content in hydrogels.[19] Several classes of hydrogels exhibit highly nonlinear behavior, and the employability of hyperelastic material models can be envisaged. Xiang et al. proposed a hyperelastic model based on entanglements in polymeric chains of hydrogels.[20] Later, this study was further used to show the effect of water content on the mechanical behavior of hydrogels.[21] The latter elaborated studies are good for the interpretation of structure−property relationships of hydrogels, which can be further improved by introducing a failure description. For example, the energy limiter introduced by Volokh has been promising to describe failure in constitutive models for several types of soft material.[22]

The phenomenon of cavitation has been widely explored for fluids, mainly water.[23,24] However, the mechanism of cavitation is not well explored for water-based solids such as hydrogels. The sophisticated experimental facilities needed to explore cavitation in hydrogels have somehow restricted these studies. The molecular structure and nonlinear elastic behavior of hydrogels make the study of cavitation even more challenging.[25,26] The recent developments in the description of failure and fracture in constitutive models have paved the path for observing the cavitation mechanism using numerical simulations.

Summarizingly, the aim of this study is to prepare imidazole−Ni^{2+}-based physically cross-linked hydrogels and their mechanical characterization. The study is followed by (1) describing failure in a classical hyperelastic material model, (2) the bulge test of hydrogels, which involves calibration of material parameters using reverse finite-element (FE) methodology, (3) structure−property relationship, and (4) exploring cavitation in hydrogels. We also analyze the effect of polymer/water content on elastic modulus and energy limiters.

EXPERIMENTAL SECTION

Materials. 1-Vinyl imidazole (VIm) and nickel(II) chloride hexahydrate were purchased from Thermo Scientific. Methacrylamide (MAAm) and ammonium persulfate (APS) were purchased from Sigma-Aldrich. *N*,*N*,*N*′,*N*′-Tetramethylethylenediamine (TEMED) was purchased from Acros Organics. Deionized water (Millipore, Merck) was used for all of the experiments. All chemicals were used as received.

Preparation of Hydrogels. The physically cross-linked hydrogels were prepared using a one-pot radical polymerization reaction. Methacrylamide (2.77 g, 3.25 M), vinyl imidazole, and nickel(II) chloride hexahydrate were added in deionized water (total volume 10 mL) and stirred vigorously at 30 °C for 30 min to dissolve. After that, the solution was vortexed for 30 min, and 1 wt % APS and 20 μL of TEMED were added. The resulting solution was poured into a Teflon mold and kept for 12 h to form a physically cross-linked hydrogel. The hydrogels were denoted as PMV-*X*-Ni, where *X* is the molar percentage of VIm with respect to MAAm (i.e., 40, 50, 60, 70%), while the molar ratio of VIm to nickel(II) chloride hexahydrate was fixed at 4:1. The water content in the hydrogels was calculated as $W_c = (w_s - w_d)/w_s$, where w_s and w_d are the weights of the hydrogel in the as-prepared and dried states, respectively.

UV−Vis Spectroscopy. A scanning spectrometer, GENESYS 10uv (Thermo Scientific), was used to measure the absorption spectra of hydrogels in the range of 300−800 nm.

Fourier Transform Infrared Spectroscopy (FTIR). FTIR measurements of air-dried hydrogel samples were performed by using a Nicolet 380 spectrometer (Thermo Fisher Scientific). The spectra were recorded in the range of 600−4000 cm^{-1}, with 64 scans averaged for each measurement.

Rheological Studies. A Discovery DHR-2 rheometer (TA Instruments) was used to examine the mechanical properties of the hydrogels under shear deformation. Parallel-plates geometry with a diameter of 20 mm and a gap of 1.4−1.6 mm was applied. Waterproof sandpaper (240 grit) was attached to the plates' surface to prevent samples from slipping during deformation. All tests were carried out at room temperature (25 °C). Amplitude sweep tests were performed at a frequency of 1 Hz. Frequency sweep tests were conducted in the frequency range of 0.1−250 rad/s at the strain amplitude of 0.1%.

Creep−recovery tests were carried out by continuous shearing at a constant stress of 3 kPa for Ni-containing hydrogels (PMV-*X*-Ni) and 300 Pa for the original PMV-40 (creep stage) with subsequent instant removal of the applied stress (recovery stage). The creep stage lasted 5 min, while the recovery stage lasted 15 min. The evolution of strain over time was recorded for each of the stages.

Bulge Tests. The bulge test refers to the inflation of soft materials/polymeric membranes, where a multiaxial state of stress is observed (equibiaxial at the very top of the inflated material). The in-house-developed bulge test device (Figure 1) is used in the current study to interpret the equibiaxial tension generated in the material. The hydrogel specimens of 3 mm thickness were clamped between the upper flange (15 mm thick) and the bottom surface of the inflator. There was a hole 30 mm in diameter to permit the inflation of the

https://doi.org/10.1021/acs.macromol.5c00486
Macromolecules 2025, 58, 4478−4487

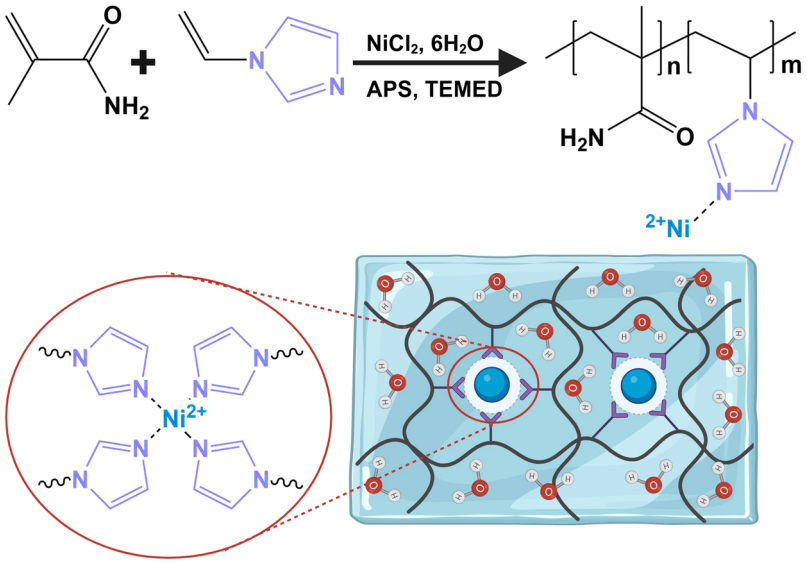

Figure 2. Synthesis scheme for the preparation of PMV-*X*-Ni hydrogels.

membrane. The pressure is supplied using a pressure flow controller at a low pressure rate of 0.02 bar/s to avoid viscoelastic effects. Later on, the supplied pressure inside the inflated membrane is recorded using a pressure transducer (0−10 bar, 0.5% accuracy). The height at the top of the inflated membrane is recorded using a laser distance sensor. All of the components used in the device were well calibrated prior to performing experiments. All of the data sets obtained from various components were saved using an in-house developed NI LabVIEW program. Four samples of each hydrogel were tested to ensure repeatability, and a significance level of 0.05 is considered while plotting the experimental data.

CONSTITUTIVE MODELING

The Helmholtz free energy per unit reference volume can be written as

$$\psi(\mathbf{F}, \zeta) = \psi_f - \mathcal{H}(\zeta)\psi_e(\mathbf{F}) \tag{1}$$

where

$$\psi_e(\mathbf{F}) = \frac{\phi}{m}\Gamma\left[\frac{1}{m}, \left(\frac{W(\mathbf{F})}{\phi}\right)^m\right], \psi_f = \psi_e(\mathbf{1}) \tag{2}$$

and $\Gamma(z, x) = \int_x^\infty t^{z-1}e^{-t}\,dt$ is the upper incomplete γ function; $\mathbf{F}$ is the deformation gradient; ψ_f and ψ_e correspond to failure energy and elastic energy; $W(\mathbf{F})$ is the strain energy function of intact material; m is a dimensionless parameter, which controls sharpness of transition to material failure; ϕ is the energy limiter; $\mathbf{1}$ is second-order identity tensor; $\mathcal{H}(\zeta)$ is the Heaviside step function, which prevents material healing: $\mathcal{H}(\zeta) = 0$ if $\zeta = 0$ and $\mathcal{H}(\zeta) = 1$, otherwise. The switch parameter $[\zeta \in (-\infty, 0)]$ is calculated using the evolution equation

$$\dot{\zeta} = -\mathcal{H}\left(\gamma - \frac{\psi_e}{\psi_f}\right), \zeta(0) = 0 \tag{3}$$

where $0 < \gamma \ll 1$ is the precision limit. We assume that the hydrogel used in the present study is nearly incompressible ($\det\mathbf{F} = 1$). We use thermodynamic reasoning explained by Volokh et al.[27] and calculate the first Piola−Kirchoff stress as

$$\mathbf{P} = \frac{\partial\psi}{\partial\mathbf{F}} - \kappa\mathbf{F}^{-T} = \exp[-(W/\phi)^m]\mathcal{H}(\zeta)\frac{\partial W}{\partial\mathbf{F}} - \kappa\mathbf{F}^{-T} \tag{4}$$

We use the Yeoh model[28,29] as the strain energy function, which is written as

$$W = \sum_{i=1}^{3} C_i(I_1 - 3)^i \tag{5}$$

where C_i are material constants and $I_1 = \mathbf{F}{:}\mathbf{F}$ is the first principal invariant. Using eqs 4 and 5, we write

$$\mathbf{P} = 2\mathcal{H}(\zeta)\exp[-(W/\phi)^m](C_1 + 2C_2(I_1 - 3) + 3C_3(I_1 - 3)^2)\mathbf{F} - \kappa\mathbf{F}^{-T} \tag{6}$$

where κ is the Lagrange multiplier, which is generally calculated using equilibrium conditions. The state of stress at the very top of the specimen during the bulge test is equibiaxial, for which the deformation gradient is written as

$$\mathbf{F} = \lambda(\mathbf{e}_1 \otimes \mathbf{e}_1 + \mathbf{e}_2 \otimes \mathbf{e}_2) + \frac{1}{\lambda^2}\mathbf{e}_3 \otimes \mathbf{e}_3 \tag{7}$$

where $\mathbf{e}_1$, $\mathbf{e}_2$, and $\mathbf{e}_3$ are Cartesian basis vectors and λ is the stretch in the axial direction. We use the above equations and write the diagonal Piola−Kirchhoff stresses as

$$P_1 = P_2 = 2\mathcal{H}(\zeta)\exp[-(W/\phi)^m]\left[C_1 + 2C_2\left(2\lambda^2 + \frac{1}{\lambda^4} - 3\right) + 3C_3\left(2\lambda^2 + \frac{1}{\lambda^4} - 3\right)^2\right]\lambda - \kappa\frac{1}{\lambda} \tag{8}$$

and

$$P_3 = 2\mathcal{H}(\zeta)\exp[-(W/\phi)^m]\left[C_1 + 2C_2\left(2\lambda^2 + \frac{1}{\lambda^4} - 3\right) + 3C_3\left(2\lambda^2 + \frac{1}{\lambda^4} - 3\right)^2\right]\frac{1}{\lambda^2} - \kappa\lambda^2 \tag{9}$$

https://doi.org/10.1021/acs.macromol.5c00486
Macromolecules 2025, 58, 4478−4487

Since there is no unloading of material, we set $\zeta \equiv 0 \Rightarrow \mathcal{H}(\zeta) \equiv 1$. We apply the equilibrium condition $P_3 = 0$ and calculate the Lagrange multiplier (κ) as

$$\kappa = 2\exp[-(W/\phi)^m]\left[C_1 + 2C_2\left(2\lambda^2 + \frac{1}{\lambda^4} - 3\right) + 3C_3\left(2\lambda^2 + \frac{1}{\lambda^4} - 3\right)^2\right]\frac{1}{\lambda^4} \quad (10)$$

Substituting κ in eq 8, we obtain

$$P = 2\exp[(W/\phi)^m]\left[C_1 + 2C_2\left(2\lambda^2 + \frac{1}{\lambda^4} - 3\right) + 3C_3\left(2\lambda^2 + \frac{1}{\lambda^4} - 3\right)^2\right]\left[\lambda - \frac{1}{\lambda^5}\right] \quad (11)$$

Furthermore, the Cauchy stress (σ) can be calculated as

$$\sigma = 2\exp[(W/\phi)^m]\left[C_1 + 2C_2\left(2\lambda^2 + \frac{1}{\lambda^4} - 3\right) + 3C_3\left(2\lambda^2 + \frac{1}{\lambda^4} - 3\right)^2\right]\left[\lambda^2 - \frac{1}{\lambda^4}\right] \quad (12)$$

RESULTS AND DISCUSSIONS

Synthesis and UV−Vis Characterization. The poly(methacrylamide-*co*-vinyl imidazole)-Ni hydrogel (denoted as PMV-*X*-Ni, where *X* represents mol % of vinyl imidazole relative to methacrylamide) was synthesized in a single step, using varying molar ratios of methacrylamide and vinyl imidazole in the presence of nickel salt (vinyl imidazole/Ni^{2+} at 4:1 ratio). The polymerization was carried out via free radical polymerization using ammonium persulfate as the initiator and TEMED as the accelerator. The synthesis scheme can be realized in Figure 2. The water content for PMV-*X*-Ni hydrogels is found to be 44, 41, 38, and 32% when *X* is 40, 50, 60, and 70%, respectively.

The coordination bond formation between imidazole and Ni^{2+} could be easily observed visually by the deep blue color of hydrogels upon the introduction of the nickel salt. The UV−vis spectra (Figure 3) of PMV-40 (prepared without metal salts) remained nearly flat in the range of 300−800 nm, while the pure PMAAm hydrogel with nickel salt showed an intense absorption peak at 393 nm and a weaker peak at 722 nm, with a shoulder at 662 nm, due to the spin−obit coupling. These characteristic absorption peaks are indicative of the octahedral $[Ni(H_2O)_6]^{2+}$ complex and further suggest that methacrylamide does not form any coordination bonds with the metal salt.[8,30] By contrast, PMV-Ni-40 exhibited absorption peaks at 370 and 605 nm, indicating a significant blue-shift due to the substitution of water (ligand) by the imidazole (ligand) in the coordination sphere of Ni^{2+}, thereby confirming the formation of the imidazole−Ni coordination bond.[8,30]

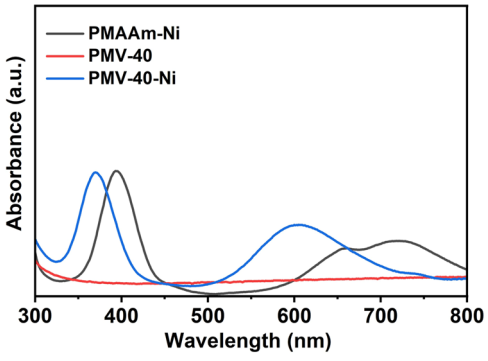

Figure 3. UV−vis spectra of the hydrogel films.

Further, FTIR spectroscopy was conducted to confirm the formation of metal−ligand interactions. The spectrum of air-dried PMV-40 hydrogel (Figure 4) exhibited a prominent peak

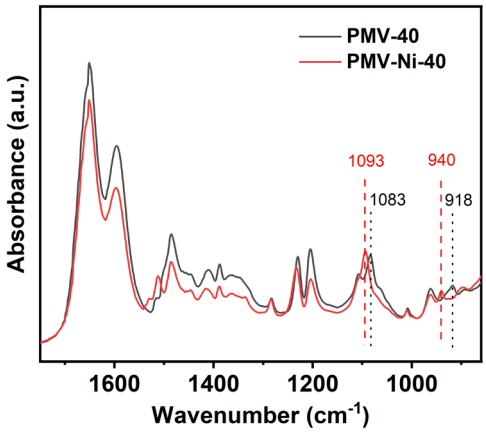

Figure 4. FTIR spectra of air-dried PMV-40 and PMV-Ni-40 hydrogels.

at 1651 cm^{-1}, corresponding to C═O (amide I), and a shoulder at 1596 cm^{-1}, attributed to CN resonance, characteristic of polymethacrylamide.[31] Distinct peaks associated with imidazole were observed at 1485 cm^{-1} (C═C and C═N stretching), 1388 cm^{-1} (ring stretching), 1230 cm^{-1} (C−H bending and C−N stretching), 1083 cm^{-1} (CH in-plane bending and ring stretching), and 918 cm^{-1} (ring mode, R_6).[32,33] The Ni^{2+}−imidazole coordination bonds could be evidenced by changes in imidazole peaks in the spectrum of PMV-40-Ni (Figure 4), including the shift of 1083 cm^{-1} (CH in-plane bending and ring stretching) to 1093 cm^{-1}, the decrease in the intensity of ring mode (R_6) at 918 cm^{-1}, and the emergence of a new band at 940 cm^{-1}.[32,33]

Mechanical Properties of the Hydrogels under Shear. The effect of imidazole−Ni^{2+} coordination cross-links on the mechanical properties of the PMV hydrogel was assessed through rheological measurements at an oscillatory shear deformation mode. The mechanical properties of PMV-40 and PMV-40-Ni hydrogels were investigated by measuring storage (G') and loss (G'') moduli as a function of oscillation frequency under a constant strain, in the region of linear viscoelastic response of the material. The characteristic relaxation time, τ_c, is defined as the inverse of the frequency at which G' equals G'' (crossover point). Above this frequency, the hydrogel exhibits solid-like behavior, storing more energy than it dissipates ($G' > G''$), while below τ_c, it demonstrates liquid-like behavior, dissipating more energy than it stores ($G'' > G'$). PMV-40 exhibited a crossover point at ∼0.4 rad/s, whereas PMV-40-Ni consistently demonstrated solid-like behavior ($G' > G''$) across the entire experimental frequency range (Figure 5a). Therefore, the crossover point of PMV-40-

https://doi.org/10.1021/acs.macromol.5c00486
Macromolecules 2025, 58, 4478−4487

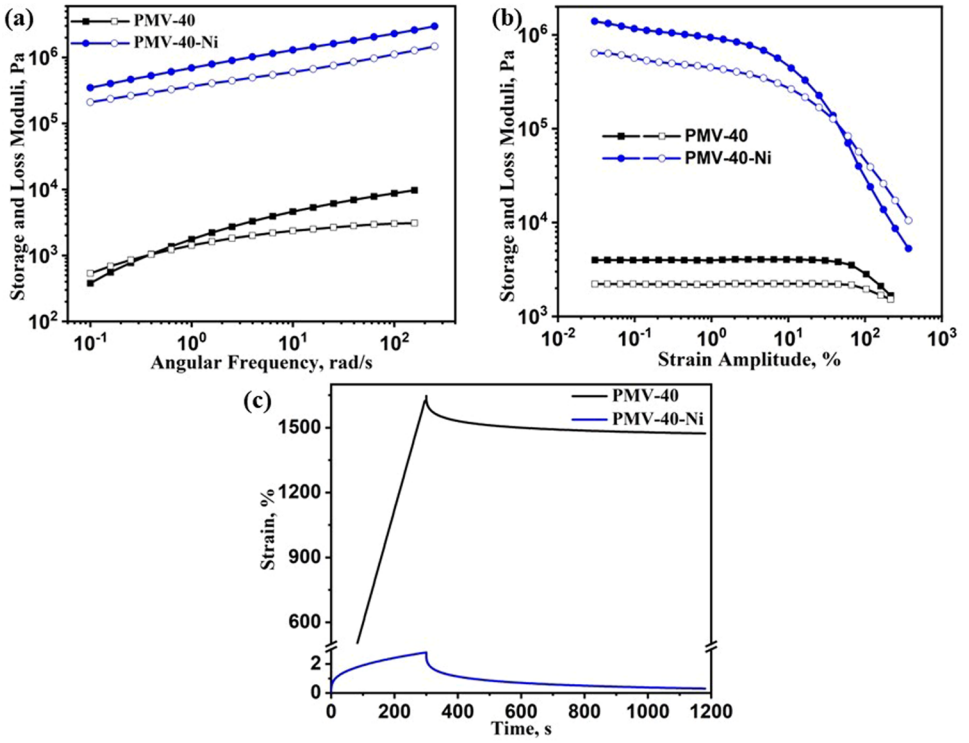

Figure 5. Storage (G') and loss (G'') moduli curves as a function of (a) frequency, (b) strain amplitude, and (c) creep−recovery for PMV-40 and PMV-40-Ni.

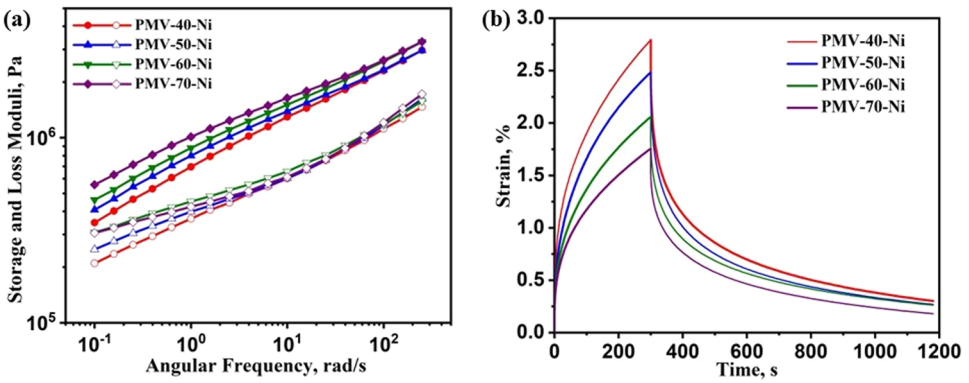

Figure 6. (a) Storage (G') and loss (G'') moduli as a function of frequency and (b) creep−recovery curves for PMV-*X*-Ni hydrogels at room temperature.

Ni shifted to lower frequencies, suggesting slower relaxation. Thus, the molecular parameters that govern τ_c are key to determining the hydrogel's ability to store and dissipate energy under dynamic mechanical force. Moreover, PMV-40-Ni exhibited significantly higher dynamic moduli, with a ∼300-fold G' increase and a ∼440-fold G'' rise (at 6.28 rad/s) when compared to PMV-40. This shows that the metal-coordination cross-links substantially promote the enhanced strength of the hydrogel. Strain amplitude sweep test further supported the PMA-40-Ni hydrogel's superior mechanical performance over PMA-40 (Figure 5b). The PMA-40 showed a more extended linear viscoelastic region, with nonlinearity occurring at higher strains than that of PMV-40-Ni. The introduction of metal-coordination bonds made PMV-40-Ni more strain-sensitive, with a crossover observed at lower strains than that of PMV-40, indicating an increased energy dissipation at higher strains. The enhanced mechanical properties of PMV-40-Ni originate from imidazole−Ni coordination cross-links acting as sacrificial bonds, preferentially breaking under load and effectively dissipating energy. Figure 5c shows the curves, presenting time-dependent behavior of the hydrogels under applied constant stress (creep) with subsequent recovery once the stress was removed. Fitting the experimental curve for PMV-40 by Burger's model[34] revealed that the steady-state viscosity and instantaneous shear modulus were ∼5.4 × 10^3 Pa·s and 2.4 kPa, respectively, while the viscoelastic modulus was 0.9 kPa. In comparison, for PMV-40-Ni, these values were much higher: 3.4 × 10^7 Pa·s, 1600, and 450 kPa, respectively. As a result, PMV-40-Ni developed a much lower strain than PMV-40 at each time point, with the difference becoming more pronounced as the creep time increased. Upon the removal of the external stress, the instantaneous (elastic) and delayed (viscoelastic) deformation recovered, while the plastic deformation did not. This separation allowed the total

https://doi.org/10.1021/acs.macromol.5c00486
Macromolecules 2025, 58, 4478−4487

deformation to be divided into reversible and irreversible components. Elastic recovery was determined as a percentage of the total deformation, and it was equal to ∼10.5% for PMV-40 and ∼89.3% for PMV-40-Ni. These results confirm that imidazole−Ni^{2+} cross-linking significantly enhances the mechanical properties of the PMV-40 hydrogel by more than 100-fold and makes it more resistant to shear deformation, with markedly improved elastic, viscoelastic, and viscous characteristics.

The influence of coordination cross-links on mechanical properties was further utilized to fine-tune the mechanical properties. Figure 6a shows G' and G'' at different frequencies of oscillating strain for the hydrogels with varying VIm/MAAm molar ratios. All hydrogels displayed a similar trend, with G' and G'' increasing linearly with frequency, characteristic of gels featuring transient mechanical cross-links.[9] In addition to that, both G' and G'' values rose progressively as the imidazole content increased, indicating the strengthening of mechanical properties. However, this enhancement was modest, so that only a ∼30% storage modulus increase was registered when the imidazole content increased from 40 up to 70%. The results of creep−recovery tests also confirmed that hydrogels with a higher imidazole content demonstrate improved mechanical properties (Figure 6b). Particularly, the parameters of Burger's model for the PMV-70-Ni hydrogel increased to ∼4.8×10^7 Pa·s and 2900 and 860 kPa for viscous, elastic, and viscoelastic components, respectively. In addition, hydrogels with increased imidazole content developed a smaller deformation under the action of applied constant stress (2.8% for PMV-40-Ni versus 1.8% for PMV-70-Ni). These results collectively establish that imidazole−Ni coordination cross-links significantly enhance the mechanical performance of the PMV hydrogel, and this enhancement can be further improved to some extent by varying the cross-linking density (by increasing the portion of the imidazole component). The latter observation motivated us to perform further mechanical investigations on PMV-*X*-Ni hydrogels.

Failure under Biaxial Tension. The structural evolution of bulge tests is elaborated in Figure 7. The structural integrity of the hydrogels used in the current study is governed by the strong physical cross-links surrounding Ni^{2+}. Macroscopically, as the pressure is increased initially, these physical cross-links restrict the deformation; however, at large pressures, the irrecoverable deformation or rupture of these cross-links allows a substantial increment in δ with a small increment in applied pressure, making the response bilinear. The latter observation is dominated by increasing the molar % of VIm. For the sake of better understanding, readers are advised to see Supporting Video (bulge test of PMV-60-Ni), where the latter observations can be realized. The results obtained using bulge tests are shown in Figure 8. For clarity, we reiterate that as the molar percentage of vinyl imidazole relative to MAAm increases, the amount of nickel salt also rises since the imidazole-to-nickel ratio remains fixed at 4:1. It is observed that with the increasing VIm molar %, the pressure at failure (P_f) increases, whereas the height at failure (δ_f) decreases. The results reflect that with a change of 30% VIm molar ratio (X varied from 40 to 70%), P_f increases by 280%, while δ_f decreases by 19%.

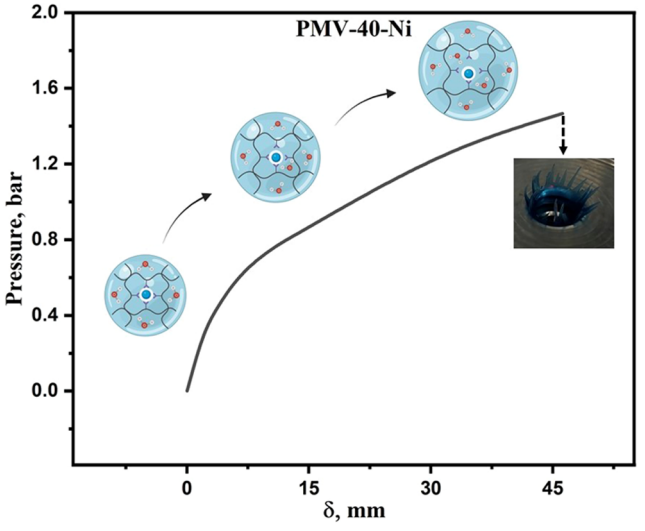

Figure 7. Structural evolution of PMV-*X*-Ni hydrogels during bulge tests. Experimental data of PMV-40-Ni is used as an example for elaboration.

The modeling and interpretation of bulge test results are not trivial due to the presence of the nonuniform state of strain throughout the inflated membrane. We opt for reverse finite-element (FE) modeling to calibrate the material parameters. The simulation and optimization are performed as per the methodology elaborated by Balakhovsky et al.[35] Simulations were performed by discretizing the hydrogel specimen into 3-noded axisymmetric shell elements (500 elements). The initial stage and boundary conditions employed in the simulations are shown in Figure 9. We constrained all of the degrees of freedom at Z, and the symmetry boundary condition was applied at X. The pressure shots are supplied at the bottom of the elements. We observed that while performing experimental investigations, when we clamp the upper flange after placing the hydrogel, the material is slightly elevated at the center of the specimen (XY). We measured the distance between X and Y by taking readings from the laser distance sensor just before and after clamping. Most often, the latter distance was ∼15 mm, which is the thickness of the upper flange.

The simulations were performed until the pressure reached P_f, and the corresponding height of the inflated membrane (δ) was noted. We used the Yeoh model (eq 5) as the strain energy function and optimized material parameters (C_1, C_2, and C_3) by minimizing the error. The simulations and optimization were performed by writing the FE code in MATLAB R2022b.[36] Later, we use these parameters to evaluate equibiaxial response at the center of the membrane and, in this sophisticated way, call it experimental equibiaxial results. The pressure versus height results obtained by simulations are shown in Figure 8 by dotted lines, and the obtained material parameters are elaborated in Table 1. The material parameters obtained are further used to evaluate the elastic modulus (E) using $E = 6C_1$, assuming the material is in the initial configuration, where $I_1 = 3$. The cross-linking density (ν) is also calculated as $\nu = E/3RT$, where R and T are the gas constant and the ambient temperature, respectively.[28,37] The cross-linking density increases with the increasing VIm content in hydrogels (Table 1).

The experimental equibiaxial results are shown in Figure 10, and the results obtained using the constitutive model including the description of failure are denoted by dotted lines. The ultimate stress (σ_u) increases with increasing the molar % of VIm at a cost of reduced critical stretch (λ_u). σ_u increased by 80% and λ_u decreased by 22% when X is varied from 40 to

https://doi.org/10.1021/acs.macromol.5c00486
Macromolecules 2025, 58, 4478−4487

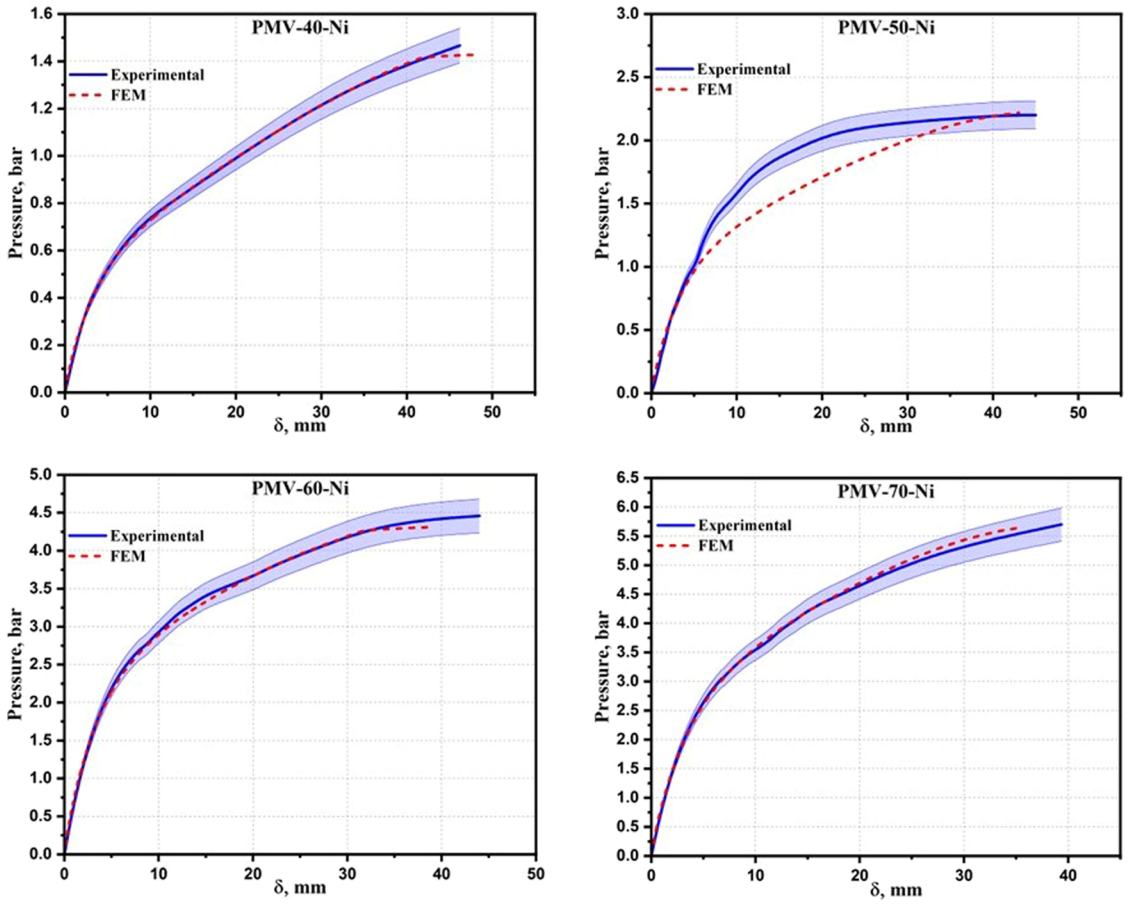

Figure 8. Pressure vs height for PMV-*X*-Ni hydrogels.

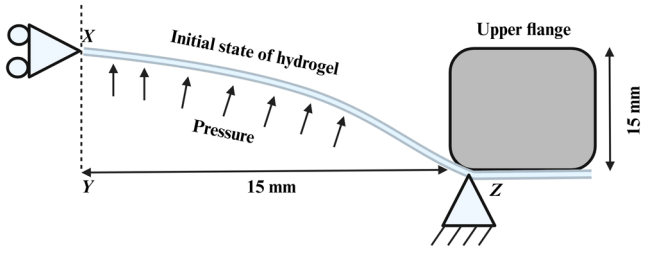

Figure 9. Initial stage of the finite-element model used for simulations.

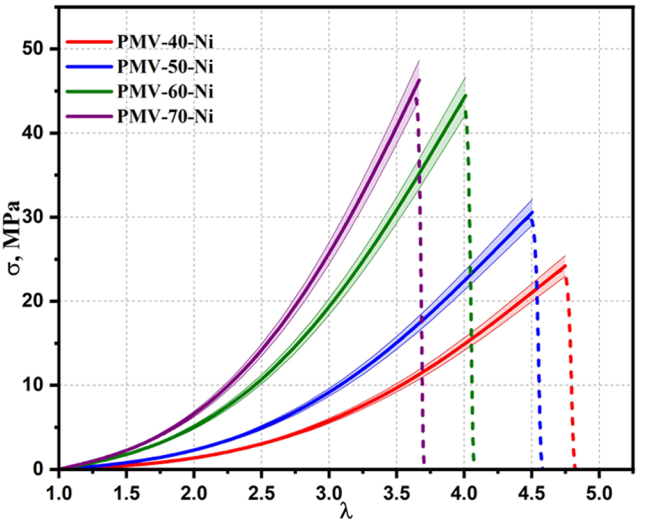

Figure 10. Equibiaxial stress vs stretch for PMV-*X*-Ni hydrogels. The dotted lines represent results acquired from theoretical modeling.

70%. The elastic modulus (E) increases with increasing X, and it is observed that it increases linearly. The latter observation justifies the linear reinforcement with an increasing molar fraction of VIm (γ_{Im}). The energy limiter ϕ increases up to γ_{Im} = 0.6 (X = 60%), and then a marginal drop is observed for γ_{Im} = 0.7 (X = 70%), where γ_{Im} is the molar fraction of VIm. It should be noted that the aforementioned findings are for $X \in$ [40, 70%]. The increment in elastic modulus with respect to γ_{Im} can be calculated using eq 13 (Figure 11a), where α =

Table 1. Constitutive Model Parameters

hydrogel	C_1, MPa	C_2, MPa	C_3, MPa	ϕ, MPa	ν, mol/m^3
PMV-40-Ni	9.59×10^{-2}	8.92×10^{-3}	-5.82×10^{-5}	16	77
PMV-50-Ni	1.75×10^{-1}	1.37×10^{-2}	-1.07×10^{-4}	21	141
PMV-60-Ni	4×10^{-1}	2.92×10^{-2}	-2.81×10^{-4}	31	322
PMV-70-Ni	4.91×10^{-1}	4.18×10^{-1}	-4.41×10^{-4}	30	396

https://doi.org/10.1021/acs.macromol.5c00486
Macromolecules 2025, 58, 4478−4487

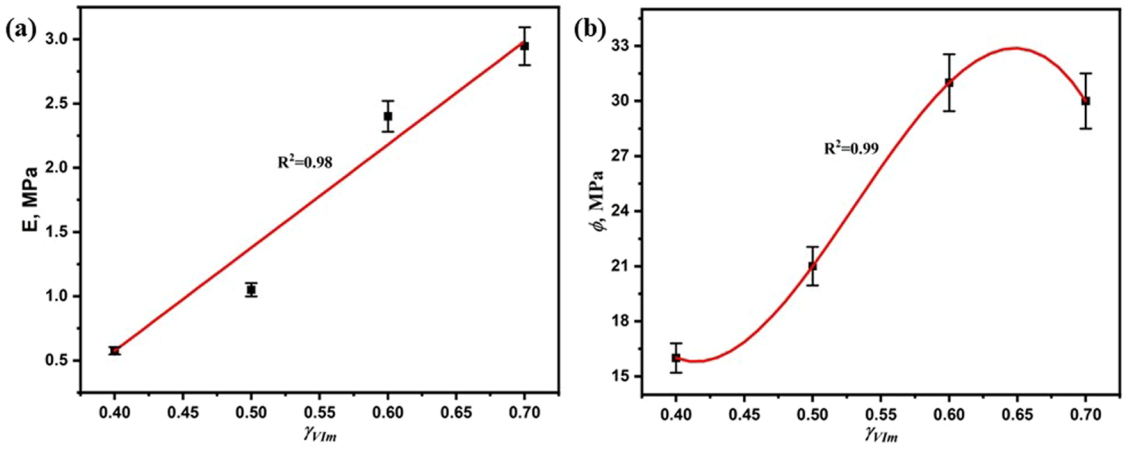

Figure 11. Variation of (a) elastic modulus and (b) energy limiter with respect to the molar fraction of VIm in PMV-*X*-Ni hydrogels.

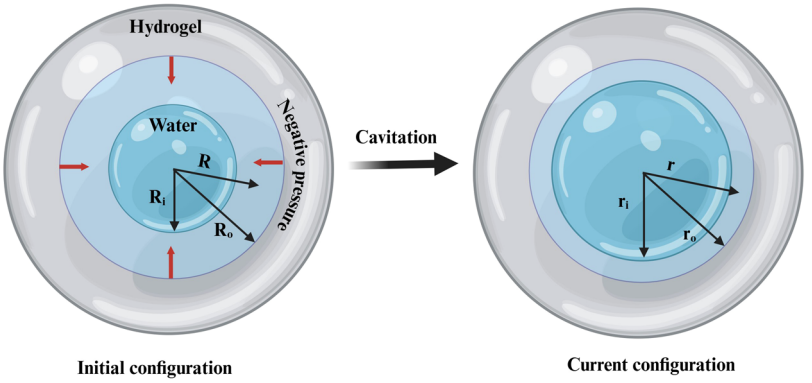

Figure 12. Process of cavitation in the hydrogels.

8.025 MPa and $E_{0.4}$ is the elastic modulus at $\gamma_{Im} = 0.4$. Similarly, using eq 14 (Figure 11b), the change in ϕ with respect to γ_{Im} can be evaluated, where β_1, β_2, β_3, and $\phi_{0.4}$ are −28.33, 1050, −2666.67 MPa, and ϕ at $\gamma_{Im} = 0.4$, respectively.

$$E = \alpha(\gamma_{Im} - 0.4) + E_{0.4} \tag{13}$$

$$\phi = \beta_1(\gamma_{Im} - 0.4) + \beta_2(\gamma_{Im} - 0.4)^2 + \beta_3(\gamma_{Im} - 0.4)^3 + \phi_{0.4},\ \gamma_{Im} \in [0.4, 0.7] \tag{14}$$

Cavitation. The mechanical deformation of hydrogels tends to introduce the so-called negative pressure, which favors the creation of microvoids by reducing intramolecular cohesive forces. In Figure 12, we elaborate on the expansion of a spherical void in the hydrogel. The hydrostatic tension (g) during cavitation can be evaluated by[17]

$$g = 2\int_x^y \left(\lambda_2 \frac{\partial \psi}{\partial \lambda_2} - \lambda_1 \frac{\partial \psi}{\partial \lambda_1}\right)\frac{\partial z}{z} \tag{15}$$

where $x = r_i/R_i$, $y = r_o/R_i$, $z = r/R_i$, $\lambda_1 = R^2/r^2$, and $\lambda_2 = r/R$.

The enhanced elastic response in stiffer hydrogel restricts the expansion of the cavity, thus lowering the critical normalized radius.[38] The critical hydrostatic tension at the onset of material instability (g_c) is proportional to the stiffness of the hydrogel.[39] The latter is the reason for increased g_c with increasing VIm molar % in hydrogel. The g_c for PMV-70-Ni is found to be ∼300% more than that of PMV-40-Ni. However, the critical normalized radius $(r_i/R_i)_c$ is observed to be ∼36% more in PMV-40-Ni when compared with PMV-70-Ni (Figure 13).

CONCLUSIONS

This study focuses on the first comprehensive evaluation of hydrogels under inflation−bulge tests, the constitutive

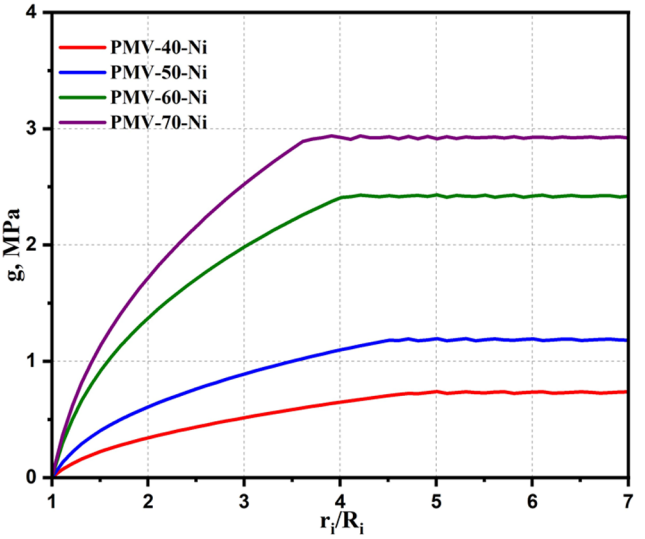

Figure 13. Variation of hydrostatic tension with respect to the normalized radius for PMV-*X*-Ni hydrogels.

https://doi.org/10.1021/acs.macromol.5c00486
Macromolecules 2025, 58, 4478−4487

modeling including description of failure and structure−property relationship. In this way, the overall mechanical response of PMV-*X*-Ni hydrogels was analyzed. Initially, a detailed study was performed to compare the mechanical properties of PMV-40 and PMV-40-Ni hydrogels. The latter comparison revealed that the hydrogels with added VIm had superior rheological and mechanical properties. The next part of the study involved a thorough investigation of mechanical properties and material modeling of PMV-*X*-Ni hydrogels.

The bulge tests revealed that increasing the VIm content in hydrogels increased the pressure at failure and decreased the bulge height at failure. During the bulge test, the physical cross-links were found to be stronger during the initial phase of the experiment, and later, the weakened physical cross-links exhibited a significant change in the expansion of the material with a marginal increment in pressure.

The developed constitutive model was calibrated using an inverse finite-element methodology-based optimization technique, and the equibiaxial response of the hydrogel was evaluated. The ultimate equibiaxial stress was enhanced by 80% when the VIm content was increased by 30%, whereas the critical stretch decreased by 22%. The empirical relationship developed for elastic modulus and energy limiter with respect to the molar fraction of VIm is helpful in optimizing the mechanical properties of PMV-*X*-Ni hydrogels as per the application. The phenomenon of cavitation is very interesting to analyze the critical hydrostatic tension for void growth, which increases with the increase in the VIm content, but at the cost of reduced critical normalized radius.

In conclusion, the studied hydrogels are potential candidate materials for use in electronics and energy storage devices. In such engineering applications, a thorough evaluation of hydrogels under a multiaxial state of stress is advised to ensure durability and fail-safe design. The developed methodologies can be helpful in thoroughly analyzing the mechanical behavior of hydrogels experimentally, and the constitutive models can be further utilized for simulation-based design optimization.

■ ASSOCIATED CONTENT

Supporting Information

The Supporting Information is available free of charge at https://pubs.acs.org/doi/10.1021/acs.macromol.5c00486.

Inflation of hydrogel (MOV)

■ AUTHOR INFORMATION

Corresponding Authors

Mohit Goswami − *Faculty of Civil and Environmental Engineering, Technion Israel Institute of Technology, Haifa 3200003, Israel;* orcid.org/0000-0003-4798-3801; Email: mohit@technion.ac.il

Agniva Dutta − *NanoEngineering Group, Faculty of Mechanical Engineering, Technion Israel Institute of Technology, Haifa 3200003, Israel*; Email: agniva.dutta@campus.technion.ac.il

Eyal Zussman − *NanoEngineering Group, Faculty of Mechanical Engineering, Technion Israel Institute of Technology, Haifa 3200003, Israel*; Email: meeyal@me.technion.ac.il

Konstantin Volokh − *Faculty of Civil and Environmental Engineering, Technion Israel Institute of Technology, Haifa 3200003, Israel*; Email: cvolokh@technion.ac.il

Authors

Rishi Kulshreshtha − *Faculty of Civil and Environmental Engineering, Technion Israel Institute of Technology, Haifa 3200003, Israel*

Gleb Vasilyev − *NanoEngineering Group, Faculty of Mechanical Engineering, Technion Israel Institute of Technology, Haifa 3200003, Israel*

Complete contact information is available at: https://pubs.acs.org/10.1021/acs.macromol.5c00486

Author Contributions

[§]M.G. and A.D. contribution equally.

Notes

The authors declare no competing financial interest.

■ ACKNOWLEDGMENTS

The support from the Israeli Ministry of Science and Technology (MOST-0005173) is gratefully acknowledged. This work was also supported by the Israel Science Foundation (ISF-394/20). Some of the illustrations were created using BioRender.com.

■ REFERENCES

(1) Tee, B.-K.; Wang, C.; Allen, R.; Bao, Z. An electrically and mechanically self-healing composite with pressure-and flexion-sensitive properties for electronic skin applications. *Nat. Nanotechnol.* **2012**, *7*, 825−832.

(2) Das, S.; Martin, P.; Vasilyev, G.; Nandi, R.; Amdursky, N.; Zussman, E. Processable, ion-conducting hydrogel for flexible electronic devices with self-healing capability. *Macromolecules* **2020**, *53*, 11130−11141.

(3) Lee, Y.; Song, W.; Sun, J.-Y. Hydrogel soft robotics. *Mater. Today Phys.* **2020**, *15*, No. 100258.

(4) Dutta, A.; Ghosal, K.; Sarkar, K.; Pradhan, D.; Das, R. K. From ultrastiff to soft materials: Exploiting dynamic metal-ligand cross-links to access polymer hydrogels combining customized mechanical performance and tailorable functions by controlling hydrogel mechanics. *Chem. Eng. J.* **2021**, *419*, No. 129528.

(5) Huang, S.; Hou, L.; Li, T.; Jiao, Y.; Wu, P. Antifreezing hydrogel electrolyte with ternary hydrogen bonding for high-performance zinc-ion batteries. *Adv. Mater.* **2022**, *34*, No. 2110140.

(6) Dutta, A.; Vasilyev, G.; Vilensky, R.; Zussman, E. Controlling spatiotemporal mechanics of globular protein-polymer hydrogel via metal-coordination interactions. *Chem. Eng. J.* **2024**, *482*, No. 148881.

(7) Lake, G. J.; Thomas, A. G. The strength of highly elastic materials. *Proc. R. Soc. London, Ser. A* **1967**, *300*, 108−119.

(8) Dutta, A.; Das, R. K. Dual Cross-Linked Hydrogels with High Strength, Toughness, and Rapid Self-Recovery Using Dynamic Metal−Ligand Interactions. *Macromol. Mater. Eng.* **2019**, *304*, No. 1900195.

(9) Sun, J.-Y.; Zhao, X.; Illeperuma, W. R.; Chaudhuri, O.; Oh, K. H.; Mooney, D. J.; Vlassak, J. J.; Suo, Z. Highly stretchable and tough hydrogels. *Nature* **2012**, *489*, 133−136.

(10) Sun, T. L.; Kurokawa, T.; Kuroda, S.; Ihsan, A. B.; Akasaki, T.; Sato, K.; Haque, M. A.; Nakajima, T.; Gong, J. P. Physical hydrogels composed of polyampholytes demonstrate high toughness and viscoelasticity. *Nat. Mater.* **2013**, *12*, 932−937.

(11) Nafo, W.; Al-Mayah, A. Characterization of PVA hydrogels' hyperelastic properties by uniaxial tension and cavity expansion tests. *Int. J. Nonlinear Mech.* **2020**, *124*, No. 103515.

(12) Nakajima, T.; Kurokawa, T.; Ahmed, S.; Wu, W.-l.; Gong, J. P. Characterization of internal fracture process of double network hydrogels under uniaxial elongation. *Soft Matter* **2013**, *9*, 1955−1966.

(13) Zhang, E.; Bai, R.; Morelle, X. P.; Suo, Z. Fatigue fracture of nearly elastic hydrogels. *Soft Matter* **2018**, *14*, 3563−3571.

(14) Wang, C.; Wiener, C. G.; Fukuto, M.; Li, R.; Yager, K. G.; Weiss, R.; Vogt, B. D. Strain rate dependent nanostructure of hydrogels with reversible hydrophobic associations during uniaxial extension. *Soft Matter* **2019**, *15*, 227−236.
(15) Lev, Y.; Faye, A.; Volokh, K. Experimental study of the effect of temperature on strength and extensibility of rubberlike materials. *Exp. Mech.* **2018**, *58*, 847−858.
(16) Lev, Y.; Faye, A.; Volokh, K. Thermoelastic deformation and failure of rubberlike materials. *J. Mech. Phys. Solids* **2019**, *122*, 538−554.
(17) Goswami, M.; Gupta, P.; Lev, Y.; Chattopadhyay, S.; Volokh, K. Multiaxial failure of dual-phase elastomeric composites. *Eng. Fract. Mech.* **2024**, *312*, No. 110625.
(18) Levin, M.; Tang, Y.; Eisenbach, C. D.; Valentine, M. T.; Cohen, N. Understanding the Response of Poly (ethylene glycol) diacrylate (PEGDA) Hydrogel Networks: A Statistical Mechanics-Based Framework. *Macromolecules* **2024**, *57*, 7074−7086.
(19) Zhong, D.; Xiang, Y.; Wang, Z.; Chen, Z.; Liu, J.; Wu, Z. L.; Xiao, R.; Qu, S.; Yang, W. A visco-hyperelastic model for hydrogels with tunable water content. *J. Mech. Phys. Solids* **2023**, *173*, No. 105206.
(20) Xiang, Y.; Zhong, D.; Wang, P.; Mao, G.; Yu, H.; Qu, S. A general constitutive model of soft elastomers. *J. Mech. Phys. Solids* **2018**, *117*, 110−122.
(21) Wang, Z.; Zhong, D.; Xiao, R.; Qu, S. Correlation between synthesis parameters and hyperelasticity of hydrogels: experimental investigation and theoretical modeling. *J. Mech. Phys. Solids* **2024**, *190*, No. 105733.
(22) Volokh, K. Hyperelasticity with softening for modeling materials failure. *J. Mech. Phys. Solids* **2007**, *55*, 2237−2264.
(23) Borkent, B. M.; Gekle, S.; Prosperetti, A.; Lohse, D. Nucleation threshold and deactivation mechanisms of nanoscopic cavitation nuclei. *Phys. Fluids* **2009**, *21*, No. 102003, DOI: 10.1063/1.3249602.
(24) Stan, C. A.; Willmott, P. R.; Stone, H. A.; Koglin, J. E.; Liang, M.; Aquila, A. L.; Robinson, J. S.; Gumerlock, K. L.; Blaj, G.; Sierra, R. G.; et al. Negative pressures and spallation in water drops subjected to nanosecond shock waves. *J. Phys. Chem. Lett.* **2016**, *7*, 2055−2062.
(25) Mahmud, K. A.; Hasan, F.; Khan, M. I.; Adnan, A. On the molecular level cavitation in soft gelatin hydrogel. *Sci. Rep.* **2020**, *10*, No. 9635.
(26) Vincent, O.; Marmottant, P.; Gonzalez-Avila, S. R.; Ando, K.; Ohl, C.-D. The fast dynamics of cavitation bubbles within water confined in elastic solids. *Soft Matter* **2014**, *10*, 1455−1461.
(27) Volokh, K. *Mechanics of Soft Materials*; Springer, 2019; Vol. *337*.
(28) Yeoh, O. H. Some forms of the strain energy function for rubber. *Rubber Chem. Technol.* **1993**, *66*, 754−771.
(29) Goswami, M.; Ghorai, S. K.; Sharma, S.; Chakraborty, G.; Chattopadhyay, S. Nonlinear fracture assessment and nanomechanical deformation of elastomeric composites: Development of finite element model and experimental validation. *Polym. Compos.* **2021**, *42*, 3572−3592.
(30) Cotton, F. A.; Wilkinson, G.; Murillo, C. A.; Bochmann, M. *Advanced Inorganic Chemistry*; John Wiley & Sons, 1999.
(31) Çavuş, S. Poly (methacrylamide-co-2-acrylamido-2-methyl-1-propanesulfonic acid) hydrogels: Investigation of pH-and temperature-dependent swelling characteristics and their characterization. *J. Polym. Sci., Part B: Polym. Phys.* **2010**, *48*, 2497−2508.
(32) Feng, W.; Zhou, W.; Zhang, S.; Fan, Y.; Yasin, A.; Yang, H. UV-controlled shape memory hydrogels triggered by photoacid generator. *RSC Adv.* **2015**, *5*, 81784−81789.
(33) Lippert, J. L.; Robertson, J.; Havens, J. R.; Tan, J. S. Structural studies of poly (N-vinylimidazole) complexes by infrared and Raman spectroscopy. *Macromolecules* **1985**, *18*, 63−67.
(34) Suriano, R.; Griffini, G.; Chiari, M.; Levi, M.; Turri, S. Rheological and mechanical behavior of polyacrylamide hydrogels chemically crosslinked with allyl agarose for two-dimensional gel electrophoresis. *J. Mech. Behav. Biomed. Mater.* **2014**, *30*, 339−346.
(35) Balakhovsky, K.; Volokh, K. Inflation and rupture of rubber membrane. *Int. J. Fract.* **2012**, *177*, 179−190.
(36) *MathWorks MATLAB version: 9.13.0 (R2022b)*, 2022.
(37) Treloar, L. G. *The Physics of Rubber Elasticity*; Oxford Press, 1975.
(38) Enrico, A.; Voulgaris, D.; Östmans, R.; Sundaravadivel, N.; Moutaux, L.; Cordier, A.; Niklaus, F.; Herland, A.; Stemme, G. 3D microvascularized tissue models by laser-based cavitation molding of collagen. *Adv. Mater.* **2022**, *34*, No. 2109823.
(39) Zimberlin, J. A.; Crosby, A. J. Water cavitation of hydrogels. *J. Polym. Sci., Part B: Polym. Phys.* **2010**, *48*, 1423−1427.

https://doi.org/10.1021/acs.macromol.5c00486
Macromolecules 2025, 58, 4478−4487